ILASS-Americas 32nd Annual Conference on Liquid Atomization and Spray Systems, May 22-25, 2022

High-fidelity multi-scale simulation of air-blast atomization with drop size comparison against experiments

Lam Vu [*], Austin Han[1], Nathanaël Machicoane[2], and Olivier Desjardins[1]
[1] Sibley School of Mechanical and Aerospace Engineering
Cornell University
Ithaca, NY 14853 USA
[2]Univ. Grenoble Alpes, CNRS, Grenoble INP, LEGI, 38000 Grenoble, France

Abstract

Air-blast atomization is a widely used spraying strategy where a high-speed gas shears and fragments a low-speed liquid, converting its kinetic energy into surface energy. Computational predictions of drop sizes in air-blast atomization present significant challenges, in part because of the wide range of length and time scales governing the process. In this work, we employ a high-fidelity multi-scale atomization modeling strategy wherein multiple simulation domains are interfaced, with each domain tackling a different length scale of the problem. Upstream, we simulate the internal gas flow of the nozzle using a fairly inexpensive single-phase solver. This generates the gas inflow conditions for a volume-of-fluid (VOF) two-phase flow simulation of the spray formation region where sheets and ligaments are shed off the liquid core, generating a large number of drops. In stand-alone VOF simulations, droplet size distributions are based off broken liquid structures, limiting the smallest drop size to be on the order of the mesh size and making such measurements strongly mesh dependent. In contrast, we use a break up model that converts thin liquid structures into spherical Lagrangian particles which are transferred to an Euler-Lagrange simulation focused on the spray dispersion region. We compare droplet statistics generated with this multi-scale spray modeling strategy against experimental measurements.

*Corresponding Author: lxv2@cornell.edu

Introduction

Sprays play an essential role in combustion systems and their effective modeling is crucial to improving surrounding technologies. Air-blast atomization is a spray strategy in which a high-speed gas destabilizes a low-speed liquid, fragmenting it into a collection of liquid ligaments and drops. These liquid structures are densely packed and dispersed in a heavily drop-mediated flow that eventually undergo evaporation and combustion. The fields of evaporation and combustion modeling are well developed (e.g. [1, 2]), while the modeling of the spray formation and break up process is limited. Specifically, few models exist that produce droplet size distributions starting from first principles. The focus of this paper is to present a modeling strategy that produces droplet distributions while modeling the atomization process from the nozzle flow to spray dispersion. This strategy has the potential to be scaled up to relevant industrial operating conditions and at a cost that remains tractable.

Computational models that produce droplet distributions range in their complexity and physical accuracy. The simplest models forgo modeling the liquid injection and break up process using the governing equations and generate drops based on phenomenological processes of surface instabilities [3, 4, 5], liquid shedding [6], and turbulence [7]. More complex models (e.g. $\Sigma - Y$, ELSA) simulate the liquid injection process but model the break up process [8, 9]. These models solve for a liquid-gas mixture, thereby bypassing the difficulty of interface tracking and related discontinuities, limiting their physicality. The highest fidelity models attempt to capture all scales of both the liquid injection and the break up process starting from the two-phase immiscible Navier-Stokes equations [10]. However, these models come at a high cost because of the small scales associated with the break up process. To put in perspective, their mesh resolutions ranged from $\Delta/h_l \approx 0.004 - 0.03$ where h_l is the height of the liquid flow passage, and used somewhere between 3 and 14 million core hours. In the present model, we simulate all scales of the liquid injection process but model the break up process, reducing the computational cost by orders of magnitude. Our study is run at realistic air-war conditions and models many of these small scales using a mesh resolution an order of magnitude larger, $\Delta/d_l \approx 0.05 - 0.1$ where d_l is liquid jet diameter, and at a cost orders of magnitude lower, between 10 and 200 thousand core hours.

In this study, we present a multi-scale simulation strategy that produces droplet distributions that are in great agreement with experimental measurements. This multi-scale strategy tackles the multi-scale nature of atomization by using blocks, with each block tackling a specific scale of the problem using its own flow solver and domain. These blocks are coupled to each other using Dirichlet boundary conditions or volumetric forcing for the velocity field, and a thin structure break up model to convert liquid structures into drops. This method of generating drops assumes that break up occurs predominantly through ruptured films. Three blocks are used to simulate the nozzle flow, spray formation, and spray dispersion processes. Drop size distributions using a standard LVIRA method and our model are compared against experiments. Results show that LVIRA exhibit heavily mesh dependent results that do not match experiments while our model is weakly mesh dependent and agrees well with experiments.

Simulation Overview

A two-fluid coaxial atomizer [11], shown in figure 1, is used in both simulations and experiments. The liquid flows through a straight circular pipe at a flow rate Q_l and separates the liquid from the coaxial gas stream that atomizes it. The gas enters the nozzle through four upstream ports perpendicular to the wall and flow through an annular passage at a total flow rate Q_{total}. U_l and U_g are the liquid and gas bulk velocities respectively, d_l is the liquid inner diameter, D_l, is the liquid outer diameter, and d_g is the gas inner diameter. The simulation is run at a gas Reynolds number, $Re_g \equiv 4Q_{Total}/\sqrt{4\pi A_g}\nu_g$, of 21400, a liquid Reynolds number, $Re_l \equiv \rho_l U_l d_l/\mu_l$, of 1200, a momentum flux ratio, $M \equiv (\rho_g U_g^2)/(\rho_l U_l^2)$, of 5.3, and a Weber number, $We \equiv \rho_g (U_g - U_l)^2 d_l/\sigma$, of 39.1 where A_g is the gas flow through area, ρ is the fluid density, μ is the dynamic viscosity, ν is the kinematic viscosity, σ is the surface tension coefficient, and subscripts l and g denote liquid and gas quantities, respectively.

Figure 2 illustrates the three aspects of the atomization process we model: the internal nozzle flow, the spray formation, and the spray dispersion region. The origin of our coordinate system is at the center of the nozzle exit. The gas nozzle flow is generated through a single phase simulation. The liquid is at a sufficiently low Re that it can be modeled as laminar pipe flow. The spray formation is simulated using a volume-of-fluid (VOF) method and a reconstruction method, R2P [12], capable of capturing liquid structures that fall below the mesh size. The spray dispersion is modeled using an Euler-Lagrange simulation where drops are dispersed and tracked as Lagrangian particles.

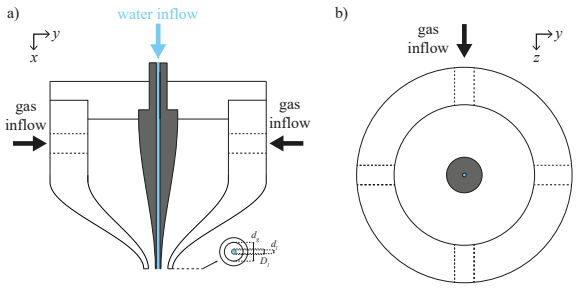

Figure 1: Nozzle schematic cut longitudinally (left) and transversely (right). Water is injected through a circular needle while gas is injected through four gas ports.

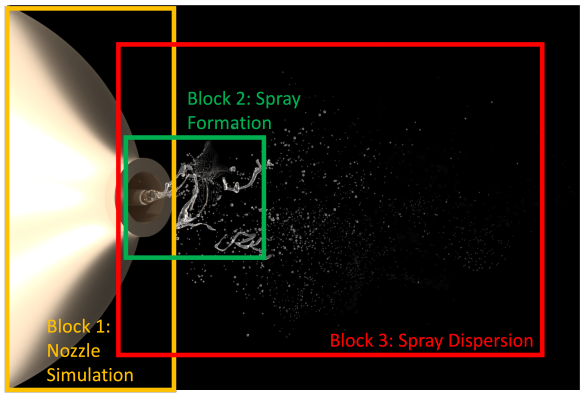

Figure 2: Illustration of three blocks modeling the nozzle flow, spray formation and spray dispersion.

In the following section, we describe the governing equations used in each block and the coupling and time stepping to synchronize the blocks.

Governing Equations

Block 1: Nozzle Flow

Co-flowing liquid and gas streams at the nozzle exit mark the beginning of the spray formation region. The liquid injection is not simulated and the gas inflow conditions are generated by a concurrent running nozzle flow simulation. The gas flows through a non-trivial nozzle geometry at a high Re and we simulate it by solving the single phase incompressible Navier-Stokes equation,

$$\begin{aligned} \nabla \cdot \boldsymbol{u} &= 0, \\ \frac{\partial u}{\partial t} + \boldsymbol{u} \cdot \nabla \boldsymbol{u} &= -\frac{1}{\rho} \nabla p + \nu \nabla^2 \boldsymbol{u}. \end{aligned} \tag{1}$$

The nozzle is stair-stepped on a Cartesian mesh and consequently, convective and viscous operators are modified. Gas is injected through lateral ports upstream in the nozzle using Dirichlet boundary conditions and all other boundary conditions are treated as a Neumann outflow. A dynamic Smagorinsky turbulence model is employed to account for subgrid scale turbulence scales [13]. The domain size is $10d_g \times 10d_g \times 10d_g$ and the mesh spacing $\Delta_1/d_g = 0.05$ is uniform in all directions. The nozzle plenum is the furthest point upstream in the domain and the furthest point downstream is d_g past the nozzle exit.

Block 2: Spray Formation

The spray formation is simulated by solving the liquid-gas flow equations for incompressible, immiscible fluids. The governing equations are

$$\begin{aligned} \nabla \cdot \boldsymbol{u} &= 0, \\ \rho \frac{\partial u}{\partial t} + \rho \boldsymbol{u} \cdot \nabla \boldsymbol{u} &= -\nabla p + \nabla \cdot (\mu [\nabla \boldsymbol{u} + \nabla \boldsymbol{u}^{\mathsf{T}}]), \\ \frac{\partial \alpha}{\partial t} + \boldsymbol{u} \cdot \nabla \alpha &= 0, \end{aligned} \tag{2}$$

with the jump conditions

$$\begin{aligned} [\![\boldsymbol{u}]\!] &= 0, \\ [\![p]\!] &= \sigma \kappa + 2 \big[\mu\big]_{\Gamma} \boldsymbol{n}^{\mathsf{T}} \cdot \nabla \boldsymbol{u} \cdot \boldsymbol{n}, \end{aligned} \tag{3}$$

where α is the liquid volume fraction in a cell, $[\![\cdot]\!]$ denotes the difference of a liquid and gas quantity across the interface and $\boldsymbol{n}$ is the interface normal. Equations (2) and (3) are solved using a geometric volume of fluid method [14]. Density and viscosity are approximated in a cell by

$$\begin{aligned} \rho &= \alpha \rho_l + (1-\alpha)\rho_g \\ \mu^{-1} &= \alpha \mu_l^{-1} + (1-\alpha)\mu_g^{-1}. \end{aligned} \tag{4}$$

In standard VOF schemes, the interface is represented in a computational cell using a single piecewise linear interface (PLIC), whose interface can be calculated using LVIRA [15]. In our simulation, we use R2P as a reconstruction method which enables thin structures to be tracked below the mesh resolution by allowing two PLICs to co-exist in a computational cell [12]. The interface curvature is calculated using paraboloid surface fits and the pressure jump is incorporated into the pressure solver using a continuum surface force approach [16]. To capture subgrid scale effects, a dynamic Smagorinsky turbulence model [13] and sub-grid scale contact line model, assuming a static contact angle of 85°, are employed [17]. The domain size is $11.16D_l \times 10D_l \times 10D_l$ and begins at $1.16D_l$ upstream of the nozzle, simulating a portion of the nozzle tip. The mesh size is uniform in all directions with a size $\Delta_2/d_l = 0.05$.

All boundary conditions are Neumann outflows except the inflow boundary where the liquid is given a parabolic velocity profile and the gas velocity is interpolated from block 1 in a time-accurate fashion.

Coupling from Block 1 to 2

Block 1 and block 2 overlap for $x \in [-1.16D_l, d_g]$. Block 1 is one-way coupled with block 2 through a velocity interpolation plane at $x = -1.16D_l$. Block 1 simulates the flow a distance d_g downstream such that the gas is aware of the expansion but not the liquid. Block 2 includes a portion of the nozzle tip to allow for flow development while simultaneously accounting for the out-flowing liquid.

Block 3: Spray Dispersion

The spray dispersion region is modeled using an Euler-Lagrange type strategy where velocity is solved on an Eulerian mesh and drops are tracked as Lagrangian particles. The governing equations are

$$\begin{aligned} \nabla \cdot \boldsymbol{u} &= 0, \\ \frac{\partial u}{\partial t} + \boldsymbol{u} \cdot \nabla \boldsymbol{u} &= -\frac{1}{\rho}\nabla p + \nu \nabla^2 \boldsymbol{u}. \end{aligned} \tag{5}$$

for the carrier phase and

$$\begin{aligned} \frac{\mathrm{D}\boldsymbol{x_p}}{\mathrm{D}t} &= \boldsymbol{u_p}, \\ \frac{\mathrm{D}\boldsymbol{u_p}}{\mathrm{D}t} &= -f_s \frac{\boldsymbol{u_{p,r}}}{\tau_p}. \end{aligned} \tag{6}$$

for the dispersed phase where $\boldsymbol{x_p}$ is the particle position, $\boldsymbol{u_p}$ is the particle velocity, $\boldsymbol{u_{p,r}} = \boldsymbol{u_p} - \boldsymbol{u}$ is the relative particle velocity. $f_s = 1 + 0.15Re_p^{0.687}$ is the Schiller-Naumann drag coefficient on the particle where $Re_p = d_p u_{p,r}/\nu_g$, τ_p is the particle Stokes response time, d_p is the particle diameter and ν_g is the gas kinematic viscosity. The domain size is $10d_g \times 10d_g \times 10d_g$ with a uniform mesh size $\Delta_3/d_g = 0.1$ and overlaps the entire domain of block 2. A Lagrangian dynamic SGS turbulence model is applied [13]. Boundary conditions are Neumann outflows in all directions.

Coupling from Block 2 to 3

Block 3 domain encompasses the entirety of block 2. Block 2 is one-way coupled with block 3 through volumetric forcing. The source term

$$\boldsymbol{S} = \frac{\boldsymbol{u_2} - \boldsymbol{u_3}}{dt}(w_x w_y w_z)^2 \tag{7}$$

where

$$\begin{aligned} w_x(x) &= \max[(L_x - x)/L_x, 0] \\ w_y(y) &= \max[2(L_y/2 - |y|)/L_y, 0] \\ w_z(z) &= \max[2(L_z/2 - |z|)/L_z, 0], \end{aligned} \tag{8}$$

is added to the gas momentum equation which puts weights near the nozzle exit. A thin structure break up model is used for block 2 to break thin liquid structures, such as films, into drops and transfer their volume to block 3 to be tracked as Lagrangian particles. This model begins by tagging and tracking coherent liquid structures, specifically films, using a connected-component labeling (CCL) algorithm [18]. The smallest thickness is monitored over time and when this thickness falls below a tolerance value, $0.01\mu m$ in this study, the break up model is executed. Starting from the smallest thickness, a running sum is kept of the liquid volume as the cells are traversed in order of increasing thickness. This continues until the running sum volume exceeds the volume of a particle that has a diameter that is a specified ratio, 10 in this study, larger than the local film thickness. At this point, the particle is created and the remaining volume from that running sum is carried forward and the process repeats until the entire film volume has been depleted. When no more particles can be created, the remaining running sum volume is evenly distributed to all particles by scaling their diameter, making this model exactly volume conserving. The particles are placed at the centroid of their respective converted film, and given the velocity of the gas at the particle location.

Time Step Synchronization

Block 2 simulates the spray formation region which poses the most difficult modeling challenge and plays the most influential role on droplet distributions. Block 1 supports block 2 with inflow conditions while block 3 cheaply enables the dispersion region to be captured. Therefore, block 2 acts as the main time driver and blocks 1 and 3 synchronize around it.

Results

Block 1's role is to yield realistic inflow conditions for block 2. As the gas velocity at the nozzle exit in the block 2 directly affects the liquid core, velocity statistics are sampled on block 2. Figure 3a show that the mean stream-wise velocity matches well against experimentally acquired hot wire data. Moreover, figure 3b shows fluctuations at the inner wall that directly impact the liquid instabilities are well predicted, while at the outer wall, where they play a secondary role, they are over-predicted.

The liquid is spatially distributed as the spray forms. Equivalent path length (EPL), the integrated liquid depth along a line of sight, is a measurement of liquid distribution. Experimentally, it can be accurately extracted through focused beam X-ray measurements [19]. Figure 4 shows the centerline EPL for simulations using LVIRA and R2P and their comparisons against experiments. The profiles show that the centerline EPL for both methods closely match each other and are in agreement with experiments. However, R2P has slightly larger values downstream likely because the method maintains the thin liquid structures that form whereas LVIRA prematurely breaks them because of numerical errors.

Figure 5 shows drop size distributions using LVIRA and R2P for two different mesh sizes and comparisons against experiments. Results show that drop size distributions using LVIRA are heavily mesh dependent, with peaks around two or three times the mesh size, and in poor agreement with experiments. R2P with our thin structure break up model show excellent agreement with experiments and exhibit a weak mesh dependence. In standard LVIRA, numerical error is the predominant cause break up and results in two-types of liquid structures than can be extracted as drops: 1) isolated flotsams below the mesh size and 2) resolved drops above the mesh size. The former is produced solely due to numerical error and the latter is produced when larger liquid structures detach through more physical mechanisms such as when the neck of a ligament undergoing a Rayleigh-Plateau instability falls below the mesh size. Therefore, we only consider drops above the mesh size and expect heavily mesh dependent results which is what we observe. In contrast, since R2P is able to maintain films below the mesh size and the break up process is modeled, we are able to limit the mesh dependency.

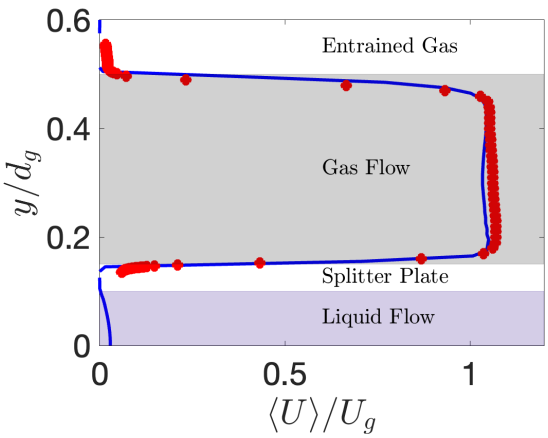

(a)

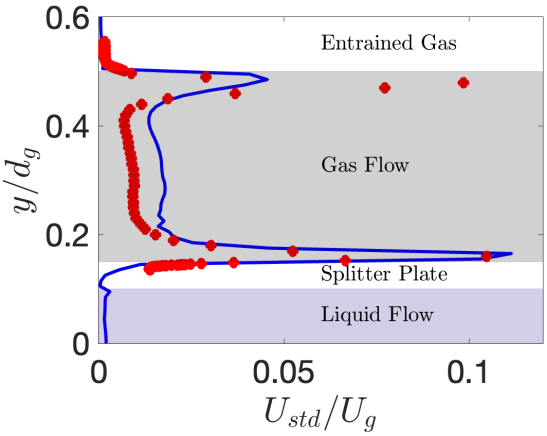

(b)

Figure 3: Comparisons of velocity statistics between the simulation (—) and experiment (•).

Conclusion

In this study, we presented a high fidelity multi-scale simulation strategy to produce drop size distributions capable of matching experiments. This multi-scale simulation strategy relies on coupled blocks, with each block tackling a different length scale of the problem. We used three blocks to model the nozzle flow, spray formation, and spray dispersion. The nozzle flow was validated by showing good experimental agreement of velocity statistics. The spray formation was validated by showing good agreement of liquid distribution statistics. Finally, we validated our break up model by showing that our method exhibited excellent agreement against droplet distribution measurements. This break up model requires tunable parameters such as the termination length scale to activate the model and the film thickness to drop diameter conversion factor. Future studies can be taken to access the dependence of these parameters on resultant drop size distributions. Moreover, better physical modeling of the thin sheets would prove useful as their development and local film size distribution at the time of break up would be more accurate, directly impacting drop size distributions.

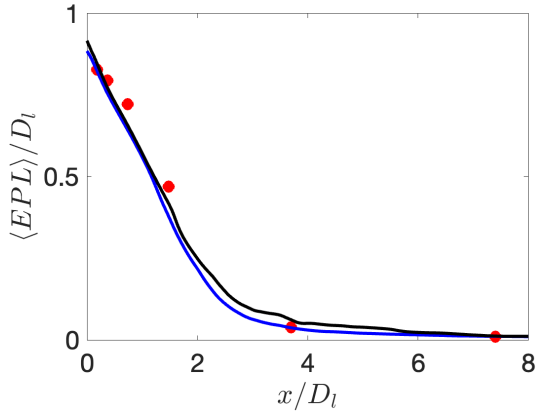

Figure 4: Comparisons of centerline EPL between LVIRA (—), R2P (—) and experiment (•).

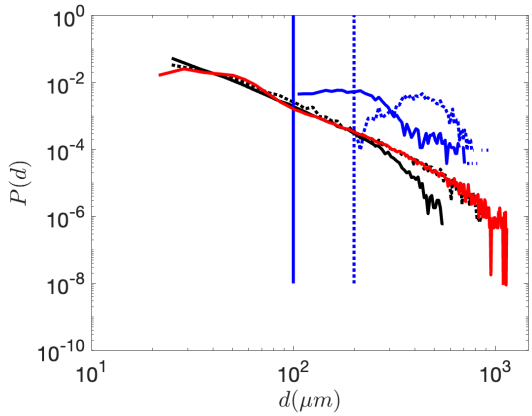

Figure 5: Comparisons of drop size distributions between LVIRA with mesh spacing $2\Delta_2$ (- -) and Δ_2 (—), R2P with mesh spacing $2\Delta_2$ (- -) and Δ_2 (—) and experiment (—). Vertical dashed and solid lines denote $2\Delta_2$ and Δ respectively.

Nomenclature

Δ	Mesh spacing
d	Inner diameter
D	Outer diameter
EPL	Equivalent path length
$\mathbf{n}$	Interface normal vector
Q	Volume flowrate
t	Time
U	Bulk Velocity
$\mathbf{u}$	Velocity
$\mathbf{x}$	Position
α	Liquid volume fraction
κ	Curvature
μ	Dynamic viscosity
ν	Kinematic viscosity
ρ	Density
σ	Surface tension

Subscripts

g	Gas
l	Liquid
p	Particle
1	Block 1
2	Block 2
3	Block 3

References

[1] Irvin Glassman, Richard A. Yetter, and Nick G. Glumac. In Irvin Glassman, Richard A. Yetter, and Nick G. Glumac, editors, *Combustion (Fifth Edition)*. Academic Press, Boston, fifth edition edition, 2015.

[2] C.K. Law. *Progress in Energy and Combustion Science*, 8(3):171–201, 1982.

[3] Rolf D. Reitz. *Atomisation Spray Technology*, 3(4):309–337, January 1987.

[4] P.J. O'Rourke and A. A. Amsden. *SAE* Paper 872089, 1987.

[5] Jennifer C. Beale and Rolf D. Reitz. *Atomization and Sprays*, 9(6):623–650, 1999.

[6] Rolf D. Reitz. *Atomization and Sprays*, 14(1), 2004.

[7] K. Y. Huh. *Proc. of The International Conf. on Multiphase Flows '91-Tsukuba*, 1991.

[8] A. Vallet and R. Borghi. *C. R. Acad. Sci. Paris Sér. II b*, 327:11015–10208, 1999.

[9] R. Lebas, T. Menard, P. A. Beau, A. Berlemont, and F. X. Demoulin. *International Journal of Multiphase Flow*, 35:247–260, 2009.

[10] Y. Ling, D. Fuster, S. Zaleski, and G. Tryggvason. *Phys. Rev. Fluids*, 2:014005, 2017.

[11] N. Machicoane, J. K. Bothell, D. Li, T. B. Morgan, T. J. Heindel, A. L. Kastengren, and A. Aliseda. *International Journal of Multiphase Flow*, 115:1–8, 2019.

[12] Robert Chiodi and Olivier Desjardins. *Journal of Computational Physics*, 449:110787, 2022.

[13] Charles Meneveau, Thomas S Lund, and William H Cabot. *Journal of Fluid Mechanics*, 319:353–385, 1996.

[14] Mark Owkes and Olivier Desjardins. *Journal of Computational Physics*, 270:587–612, 2014.

[15] James Edward Pilliod and Elbridge Gerry Puckett. *Journal of Computational Physics*, 199(2):465–502, 2004.

[16] S. Popinet and S. Zaleski. *Int. J. Numer. Meth. Fluids*, 30:775–793, 1999.

[17] Sheng Wang and Olivier Desjardins. *International Journal of Multiphase Flows*, 101:35–46, 2018.

[18] Austin Han and Olivier Desjardins. *ICLASS 2021, 15th Triennial International Conference on Liquid Atomization and Spray Systems*, Edinburgh, UK, August 29 - September 2, 2021, 2021.

[19] Julie K. Bothell, Nathanael Machicoane, Danyu Li, Timothy B. Morgan, Alberto Aliseda, Alan L. Kastengren, and Theodore J. Heindel. *International Journal of Multiphase Flow*, 125:103–219, 2020.